THE JOURNAL OF BIOLOGICAL CHEMISTRY
Vol. 273, No. 1, Issue of January 2, pp. 167–176, 1998

Printed in U.S.A.

Control of the Structural Stability of the Tubulin Dimer by One High Affinity Bound Magnesium Ion at Nucleotide N-site*

(Received for publication, September 10, 1997, and in revised form, October 27, 1997)

Margarita Menéndez‡, Germán Rivas§, J. Fernando Díaz§, and José M. Andreu§¶

From the ‡Instituto de Química Física and §Centro de Investigaciones Biológicas, Consejo Superior de Investigaciones Científicas, 28006 Madrid, Spain

Tubulin liganded with GTP at the N-site in the α-subunit and with GDP at the E-site in the β-subunit (GDP-tubulin) reversibly binds one high affinity Mg^{2+} cation ($K_b = 1.1 \times 10^7$ M^{-1}), whereas tubulin liganded with GTP at both subunits (GTP-tubulin) binds one more high affinity Mg^{2+}. The two cation binding loci are identified as nucleotide sites N and E, respectively. Mg^{2+} at the N-site controls the stability and structure of the αβ-tubulin dimer. Mg^{2+} dissociation is followed by the slow release of bound nucleotide and functional inactivation. Mg^{2+} bound to the N-site significantly increases the thermal stability of the GDP-tubulin dimer (by 10 °C and ~50 kcal mol^{-1} of experimental enthalpy change). However, the thermal stability of Mg^{2+}-liganded GDP- and GTP-tubulin is the same. Mg^{2+} binding to the N-site is linked to the αβ-dimer formation. The binding of Mg^{2+} to the α-subunit communicates a marked enhancement of fluorescence to a colchicine analogue bound to the β-subunit. Colchicine, in turn, thermally stabilizes Mg^{2+}-depleted tubulin. The tubulin properties described would be simply explained if the N-site and the colchicine site are at the α-β dimerization interface. It follows that the E-site would be at the β-end of the tubulin dimer, consistent with the known functional role of the E nucleotide γ-phosphate and coordinated cation controlling microtubule stability.

Tubulins are GTP-binding proteins that play central roles in eukaryotic cell division and organization. The αβ-tubulin dimers reversibly assemble to form the microtubules. The closest relatives of tubulins are the predicted homologous bacterial cell division FtsZ proteins (1). The GTP bound to the β-subunit is exchangeable in the dimer (E-site[1]; Ref. 2), and is hydrolyzed to GDP and P_i as a result of microtubule formation. The nucleotide γ-phosphate and a coordinated Mg^{2+} ion control the assembly activity of tubulin and microtubule stability (3–6). Tubulin with GDP in the β-subunit (GDP-tubulin) is unable to assemble into microtubules except by ligand binding to the paclitaxel site (7). GDP-tubulin is in an inactive conformation (8, 9) which favors curved assembly into double rings corresponding to pairs of curved protofilament segments (10, 11), and the curling of exposed protofilaments at microtubule ends (12, 13). In contrast to β-tubulin, the molecule of GTP bound to the α-subunit is considered non-exchangeable (N-site; Ref. 2), stays essentially bound during the entire life of the protein suggesting that it may be a structural cofactor of tubulin (14), and is coordinated to a slowly dissociating divalent cation (4).

Magnesium ions have a well established influence on tubulin-nucleotide interactions (3, 4, 15, 16) and on tubulin self-association (17, 18), including microtubule assembly (19). Equilibration in Mg^{2+}-free buffers results in a partial release of the GTP bound, followed by an irreversible loss of activity (4, 20). Previous studies of divalent cation binding (3, 4, 17, 21, 22) indicated that tubulin has two classes of Mg^{2+} binding sites, one of high affinity (with an association binding constant, $K_{1,Mg}$, in the order of 10^6 M^{-1}) and the other of low affinity ($K_{2,Mg}$, 10^2 to 10^3 M^{-1}). The stoichiometry of the first class of sites depends on the nucleotide bound to the E-site; GTP-tubulin has two tightly bound Mg^{2+} (at the N- and E-sites), whereas GDP-tubulin has a single high affinity Mg^{2+} (N-site; the E-site becomes low affinity (see Ref. 3)). This has been confirmed by studying the binding of Mg^{2+} to tubulin having GTP, GDP, or no nucleotide at the exchangeable site of the β-subunit and one Mg^{2+} ion already bound (23). The low affinity Mg^{2+} binding sites are involved in tubulin polymerization (19) and in the equilibrium association of the αβ-dimer (8). In contrast, neither the high affinity binding of Mg^{2+} to the N-site nor its intriguing role are well understood (3, 4, 23, 24).

The present study aims to understand the specific roles of the respective Mg^{2+} ions coordinated with the GTP bound to E- and N-sites in tubulin stability, structure and function. Toward these purposes, the isotherm of binding of Mg^{2+} to the N-site has been measured, and the different effects of the high affinity cations bound to GDP- and GTP-tubulin have been compared employing DSC, CD, fluorescence, and sedimentation equilibrium methods. It will be shown that the functional microtubule-stabilizing cation and γ-phosphate at the E-site impart negligible stabilization to the αβ-tubulin dimer, whereas the non-functional cation bound to the N-site, at the α-subunit, is essential for tubulin stability, and communicates with the colchicine site at the β-subunit.

EXPERIMENTAL PROCEDURES

Preparation of calf brain tubulin, without (GDP-tubulin) or with (GTP-tubulin) a γ-phosphate at the E-site was performed as described in Ref. 7, with minor modifications. GDP-tubulin was finally equilibrated in PEDTA buffer with 1 mM GDP by chromatography in Sephadex G-25 columns (10 or 25 × 0.9 cm). To prepare GTP-tubulin, 1 mM GTP and Mg^{2+} were added to GDP-tubulin. In the experiments at the lower free Mg^{2+} concentration, the EDTA concentration in the buffer was 2 mM. Nucleotides and Mg^{2+} quantification by high performance

* This work was supported by Direccion General de Ensetranse Superior Grants PB93-0114 (to M. M.), PB95-0120 (to G. R.), and PB95-0116 (to J. M. A.). The costs of publication of this article were defrayed in part by the payment of page charges. This article must therefore be hereby marked "*advertisement*" in accordance with 18 U.S.C. Section 1734 solely to indicate this fact.

¶ To whom correspondence should be addressed: Centro de Investigaciones Biológicas, Consejo Superior de Investigaciones Científicas, Velázquez 144, 28006 Madrid, Spain. Fax: 34-1-2627518; E-mail: cibjm07@cc.csic.es.

[1] The abbreviations and trivial names used are: E-site, exchangeable nucleotide binding site of tubulin; N-site, non-exchangeable nucleotide binding site of tubulin; DSC, differential scanning calorimetry; CD, circular dichroism; MTC, 2-methoxy-5-(2,3,4-trimethoxyphenyl)-2,4,6-cycloheptatrien-1-one; PEDTA, 10 mM phosphate buffer containing 1 mM EDTA, pH 7.0; paclitaxel, 4,10-diacetoxy-2α-(benzoyloxy)-5β,20-epoxy-1,7β-dihydroxy-9-oxotax-11-en-13α-y1(2*R*,3*S*)-3-[(phenylcarbonyl)-amino]-2-hydroxy-3-phenylpropionate.

liquid chromatography and atomic absorption spectrometry, respectively, and microtubule assembly were performed as described (7, 25), unless otherwise indicated. Fresh MilliQ grade water was employed to prepare all the solutions, as well as plasticware containers; any glassware material was rinsed with PEDTA buffer before use.

Binding of Mg^{2+} to Tubulin—The binding of Mg^{2+} was measured as follows. Aliquots of 200 μl of tubulin (15 μM) with a known total Mg^{2+} concentration were incubated at 10 °C for 30 min and centrifuged at 100,000 rpm for 1 h in a TLA-100 rotor, using a TLX-120 ultracentrifuge (Beckman Instruments Inc.). After centrifugation, the lower half of the tubes, which contain tubulin in equilibrium with free Mg^{2+}, and the upper half, with cation and essentially no protein, were carefully withdrawn, and the total Mg^{2+} concentration was determined in both halves. Mg^{2+} bound to tubulin was quantified by the difference in the cation concentration between the lower and the upper parts of the centrifuge tube. Free Mg^{2+} was calculated from the total Mg^{2+} concentration in the upper half, by solving the multiple equilibria, which take into account the cation binding to phosphate, nucleotide, and EDTA. The stability constants for Mg^{2+} complexes at pH 7.0 employed were as follows: phosphate, 68 M^{-1} (26, 27); GDP, 607 M^{-1} (3); GTP, 2830 M^{-1} (3); and EDTA, 2.5×10^5 M^{-1} (28). These values are within 5% variation with respect to other constants reported in the literature (26, 29–32). This, together with the calculated errors in the measurement of the total amount of Mg^{2+}, resulted in an estimated uncertainty of 10–15% for the lower calculated free Mg^{2+} concentrations, and less than 10% for the higher concentrations. Note that, in the buffer solution employed, the small free Mg^{2+} concentration approximates the mean ionic activity of $MgCl_2$ within experimental error.

A model of ligand binding assuming multiple classes of independent binding sites for Mg^{2+} (33) in the tubulin molecule was fitted to the experimental data, using a non-linear least squares procedure, based on the modified Nelder-Mead simplex algorithm (34).

Time Course of Tubulin Inactivation—The effect of Mg^{2+} on the kinetics of tubulin inactivation at constant temperature was followed by monitoring two independent properties: (i) the loss of the assembly capacity of tubulin (20 μM) with paclitaxel, monitored turbidimetrically (7) and (ii) the loss of colchicine binding sites, measured from the fluorescence of the MTC-tubulin complex (see below). Before measurement, samples were supplemented to final total Mg^{2+} concentrations of 7 and 5 mM in the assembly and MTC binding buffers, respectively. Control experiments were run in parallel at 7 mM Mg^{2+} in the initial equilibration buffer.

Circular Dichroism—The far-UV CD spectra of tubulin (1–5 μM, equilibrated in PEDTA with 1 mM nucleotide and a known amount of Mg^{2+}) were acquired in a JASCO J720 dichrograph equipped with a temperature regulated cell holder (1, 35), with a 0.1-cm cell at 20 ± 1 °C. Thermal denaturation was monitored following the variation in ellipticity at 220 nm, using a temperature scan rate of 0.5 °C·min^{-1}. Changes in secondary structure were estimated by deconvolution of the CD spectra using Yang (36), LIMCOMB, and CCA (37, 38) methods.

Fluorescence of the MTC-Tubulin Complex—The effect of Mg^{2+} on the fluorescence spectrum of the colchicine analog MTC (50 μM total concentration) bound to tubulin (5 μM) was measured essentially as described (39), using a Shimadzu RF-540 spectrofluorimeter (Kyoto, Japan; λ_{ex} = 350 nm, λ_{em} = 423 nm). The fluorescence cell (5 × 10 mm) was mounted on a holder thermostated with a water bath at 20 °C. The free and bound ligand were measured with the same high speed centrifugation method described for Mg^{2+} binding, except that MTC was measured spectrophotometrically ($\epsilon_{343} = (1.76 \pm 0.01) \times 10^4$ M^{-1} cm^{-1}) (39).

Analytical Ultracentrifugation—The measurements were performed at 10 °C with a Beckman Optima XL-A analytical ultracentrifuge equipped with absorbance optics, using an An60Ti rotor and either 12-mm double sector or six-channel centerpieces. Tubulin samples (loading concentrations between 0.5 and 15 μM) were equilibrated in PEDTA, 20 μM nucleotide, with the desired amount of Mg^{2+}. Short column (40–50 μl) sedimentation equilibrium was performed either at low speed (30 min at 30,000 rpm, followed by 2–3 h at 15,000 rpm) or as described (40): 1 h at 32,000 rpm, followed by 1–2 h at 26,000 rpm, which permitted attainment of equilibrium. Absorbance scans were taken at the appropriate wavelength (230, 275, or 290 nm). In all cases, base-line offsets were determined subsequently by high speed sedimentation. Whole-cell apparent weight-average molecular masses ($M^{c}_{w,a}$) were obtained using the programs XLAEQ and EQASSOC (supplied by Beckman; see Ref. 41). The partial specific volume was 0.736 cm^3/g (42), which was corrected for temperature (43).

To determine the equilibrium constant for tubulin dimerization (K_2), two different methodologies were employed. (i) Equilibrium association models were globally fitted to multiple sedimentation equilibrium data using either the MicroCal-Origin version of NONLIN (44) or the programs MULTEQ1B and MULTEQ3B based on the conservation of signal algorithm (41). A value of 1.16 ml mg^{-1} cm^{-1} was used for the extinction coefficient of tubulin at 275 nm in phosphate buffer (45), and the subunit relative molecular mass was taken as 55,000 (46). (ii) The dependence of the apparent weight-average molecular mass ($M_{w,a}$) on protein concentration was calculated from the local slopes of transformed data (ln*C versus* r^2) at defined radial distance intervals, using the program MWPLOTZ (kindly supplied by A. Minton, National Institutes of Health, Bethesda, MD). In this study, the $M_{w,a}$ values were calculated by superimposing data obtained from different loading protein concentrations and averaging over a concentration interval of ±0.1 log units. Models for self-association (47, 48) were fitted to the $M_{w,a}$ *versus* concentration data using a non-linear least-squares method (34).

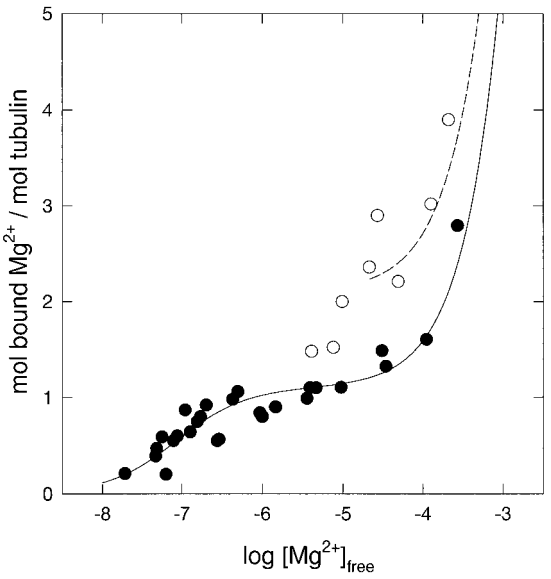

FIG. 1. **Binding of Mg^{2+} to GDP-tubulin (*solid circles*) and GTP-tubulin (*open circles*).** *Solid line*, binding isotherm calculated assuming a simple binding model ($n_{1,Mg} = 1.1 \pm 0.2$, $K_{1,Mg} = (1.1 \pm 0.3) \times 10^7$ M^{-1} plus the low affinity sites $n_{2,Mg} = 48$, $K_{2,Mg} = 106$ M^{-1} described by Frigon and Timasheff (17); see the text for details). *Dashed line*, Mg^{2+} binding values obtained by adding one to the GDP-tubulin isotherm (*solid line*) in the interval indicated.

Sedimentation velocity experiments were performed at 42,000 and 60,000 rpm. Sedimentation coefficients were calculated from the rate of the movement of (i) the solute boundary (with XLAVEL, Beckman) or (ii) the second moment of the boundary (with VELGAMMA, Beckman), and (iii) from the distribution of the apparent sedimentation coefficients, $g(s^*)$, using the DCDT program (49, 50). The sedimentation coefficients were corrected to standard conditions (51) to get the corresponding $s_{20,w}$ values.

Differential Scanning Calorimetry—The heat capacity measurements were performed in a MicroCal MC2 differential scanning calorimeter, as described previously (52). Tubulin samples (15 μM) for DSC were equilibrated in PEDTA buffer with 1 mM GDP (or GTP) and the desired Mg^{2+} concentration. The scanning rate was 0.5 °C min^{-1}, unless otherwise stated. The reversibility of thermal transitions was checked by reheating the samples after the first scan. The influence of scanning conditions on the profiles of the calorimetric transitions of tubulin was checked by running samples at several rates. The kinetic analysis of the DSC curves was carried out as described (53, 54).

RESULTS AND DISCUSSION

The thermal stability of GDP- and GTP-tubulin measured by DSC was found to be similar at free Mg^{2+} concentrations above 1 μM. However, it was dramatically reduced at the low activity of Mg^{2+} ions of the EDTA containing buffer employed for nucleotide exchange (7). This prompted an in-depth examination of the system by means of the following complementary biochemical and DSC experiments.

Binding of Mg^{2+} to GDP- and GTP-tubulin—The binding isotherms of Mg^{2+} to GDP- and GTP-tubulin in PEDTA buffer at 10 °C were directly determined by high speed sedimentation of the protein (Fig. 1). The experimental data for GDP-tubulin

TABLE I
Effect of Mg^{2+} on nucleotide content of tubulin

$[Mg^{2+}]_{free}$	*t*	GXP/tubulin	GTP/tubulin	GDP/tubulin	Mg^{2+}/tubulin
	min				
45 nM	30	1.5	0.6	0.9	0.4
45 nM	300	1.2	0.5	0.7	ND[a]
62 nM	30	1.6	0.7	0.9	0.6
62 nM	120	1.4	0.6	0.8	0.6
62 nM	300	1.3	0.6	0.7	ND
5 μM	30	1.8	0.9	0.9	1.0
50 μM	30	1.8	0.8	1.0	1.1

[a] Not determined.

can be described assuming two classes of independent binding sites in the αβ-tubulin dimer: one Mg^{2+} high affinity site ($n_{1,Mg}$ = 1.1 ± 0.2; $K_{1,Mg}$ = (1.1 ± 0.3) × 10^7 M^{-1}), plus several low affinity sites ($n_{2,Mg}$ = 48, $K_{2,Mg}$ = 106 M^{-1}; the latter values were taken from Frigon and Timasheff (17) and constrained in the fitting procedure). Measurements of samples incubated for an extra 1–2-h period at the lower ligand concentrations were essentially identical, indicating equilibrium. High affinity Mg^{2+} binding to tubulin is reversible, since supplementing cation-depleted tubulin (equilibrated in 40 ± 5 nM free Mg^{2+}) to 360 ± 20 nM free Mg^{2+} increased binding from 0.4 ± 0.1 to 0.75 ± 0.1 Mg^{2+} per tubulin heterodimer, which is within the experimental error of the reference isotherm (Fig. 1).

GTP-tubulin has one more Mg^{2+} binding site (Fig. 1, *empty symbols*) than GDP-tubulin, with an *apparent* affinity in the order of 10^5 M^{-1}. The analysis of its Mg^{2+} binding isotherm is complicated by the presence of GDP, which has a much higher affinity than GTP for the tubulin E-site at low Mg^{2+}concentration (3, 4). Therefore, as the cation concentration decreases, GDP progressively exchanges into the GTP-tubulin samples. GTP-tubulin in 63 μM free Mg^{2+} had a measured nucleotide content (0.1 GDP and 1.7 GTP per tubulin molecule), corresponding to a 90% of GTP-tubulin, and its stoichiometry of binding of Mg^{2+} is one more cation than that of GDP-tubulin. On the other hand, at 3.2 μM free Mg^{2+} the binding stoichiometry is slightly higher than 1, but the nucleotide content (0.7 GDP and 1.2 GTP per tubulin molecule) indicates that only 25% of the protein is GTP-tubulin. The results are compatible with the partial Mg^{2+} binding data of Mejillano and Himes (23) in a different buffer.

These high affinity Mg^{2+} binding sites of tubulin, one in GDP-tubulin and two in GTP-tubulin, have been previously identified as the cation-binding loci at the N and E GTP-binding sites in α- and β-tubulin, respectively (3, 4, 24). However, binding isotherm of the highest affinity Mg^{2+} to the N-site had not been measured; nor had cation-depleted tubulin been studied.

Effect of Mg^{2+} Depletion on Nucleotide Release from Tubulin—Equilibration of tubulin in Mg^{2+} free buffers results in a decrease in bound nucleotide, supposedly coming from either nucleotide dissociation from the E-site or from the irreversible protein denaturation which occurs for prolonged incubation times (4, 20). To know the role of the Mg^{2+} cation bound to the N-site of GDP-tubulin in nucleotide binding, and to identify the sites from which nucleotide may come off by cation removal, the GDP and GTP bound to tubulin were determined as a function of the free Mg^{2+} and incubation time (see Table I for a summary). Tubulin samples with the high affinity Mg^{2+} site saturated contain close to one GTP and one GDP per αβ-dimer. However, samples partially depleted from the high affinity cation have their nucleotide content reduced to 0.6–0.7 GTP and 0.9 GDP per heterodimer at the conclusion of sample preparation (an equivalent time of 0.5 h). Upon prolonged incubation at 20 °C, the GTP (and GDP) stoichiometry decreased more slowly, to values approaching the Mg^{2+}/tubulin stoichiometry of the samples (Table I). These results indicate that dissociation of Mg^{2+} from the N-site (α-subunit), which is quite reversible at short periods of time as shown above, results in dissociation of GTP (and GDP), supposedly coming from the N-site (and the E-site, respectively). This reveals the instability of the cation-depleted tubulin. The results suggest the possibility that the nucleotide binding capacity and, hence, the functionality of the β-subunit in the αβ-dimer is controlled by the cation ligation state of the α-subunit, and will be further addressed later.

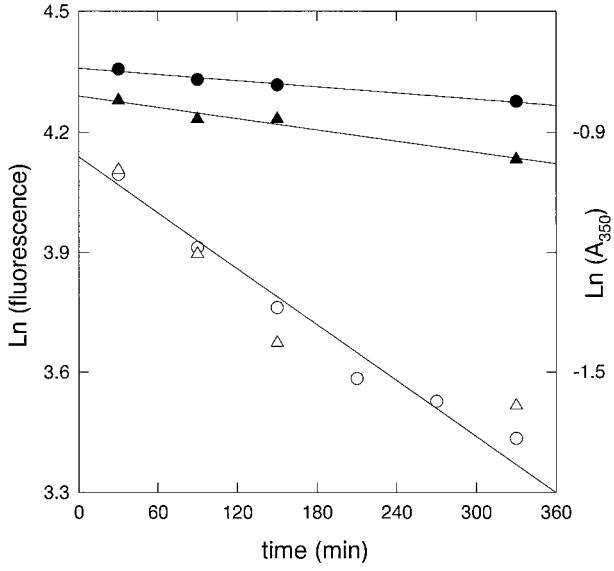

FIG. 2. **Kinetics of GDP-tubulin inactivation at 20 °C, followed by either fluorescence of the MTC-tubulin complex (*circles*) or Taxol®-induced microtubule assembly (*triangles*).** *Closed symbols* correspond to samples equilibrated at ~0.1 mM free Mg^{2+}, whereas data in *open symbols* were taken at 60 nM free Mg^{2+}. The *lines* correspond to first order kinetic rate constants of 4.6 × 10^{-6} s^{-1} (*closed circles*), 3.8 × 10^{-6} s^{-1} (*closed triangles*), and 4 × 10^{-5} s^{-1} (*open circles*).

GDP-tubulin equilibrated at 55 nM free Mg^{2+} and re-equilibrated in 6 mM $MgCl_2$ and 1 mM GTP polymerized in 3.4 M glycerol-containing buffer with a critical concentration (15 μM) 1.7 times higher than that of a GTP-tubulin control directly equilibrated in 6 mM $MgCl_2$ (9 μM). The slope of the plot of plateau turbidity *versus* total protein concentration was about 1.3 times lower than that of the control (data not shown). Since GDP-tubulin is unable to assemble in Mg^{2+}-glycerol buffer (7), this implies that around 70 ± 10% of the Mg^{2+}-depleted protein has been able to back-exchange GTP and reassemble. This result also suggests that nucleotide dissociation during the time of cation depletion of tubulin results in an irreversible conformational change, preventing the subsequent binding of nucleotide to a fraction of α- and β-subunits.

The Kinetics of Tubulin Inactivation Depends on Mg^{2+} Activity—The role of Mg^{2+} bound to the N-site on tubulin inactivation at 20 °C was investigated monitoring the time courses for the decay of paclitaxol-induced assembly, and for the binding of the colchicine analogue MTC to GDP-tubulin, at different free Mg^{2+} concentrations. GDP-tubulin equilibrated in 60 nM free Mg^{2+} initially retains more than 80% of the corresponding activity at higher cation concentrations. However, its inactivation is more rapid (half-life, $t_{½}$ = 5 h; Fig. 2) than at 300 nM free Mg^{2+} ($t_{½}$ = 7 h; data not shown), and much faster than at 100 μM free Mg^{2+} (estimated $t_{½}$ ~ 47 h; Fig. 2), compatible with previous measurements of tubulin aging (20, 55). For practical purposes, the kinetics after the initial decay can be apparently described by first order reactions, whose rate constants, *k*,

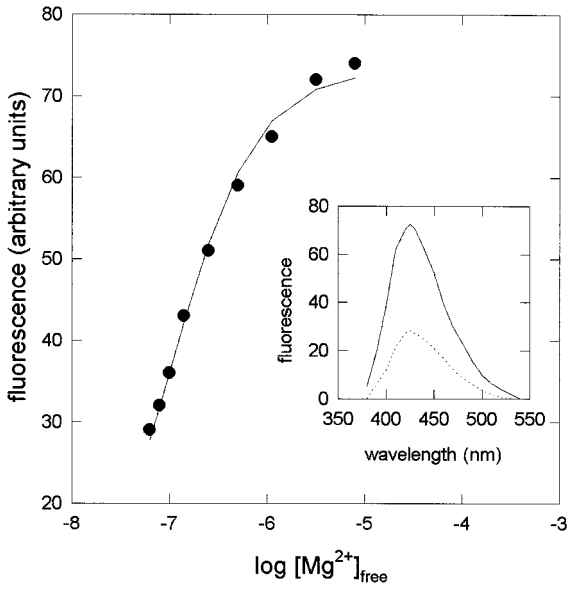

FIG. 3. **Effect of Mg^{2+} on the fluorescence intensity of the tubulin-MTC complex (5 μM) at 20 °C.** The line is a fluorescence titration curve calculated for cation-binding to a single site (F_{max} = 71, F_{min} = 8, $K_b = 9 \times 10^6$ M^{-1}). *Inset*, fluorescence spectra of the complex at 8 μM (*solid line*) and 65 nM (*dotted line*) free Mg^2.

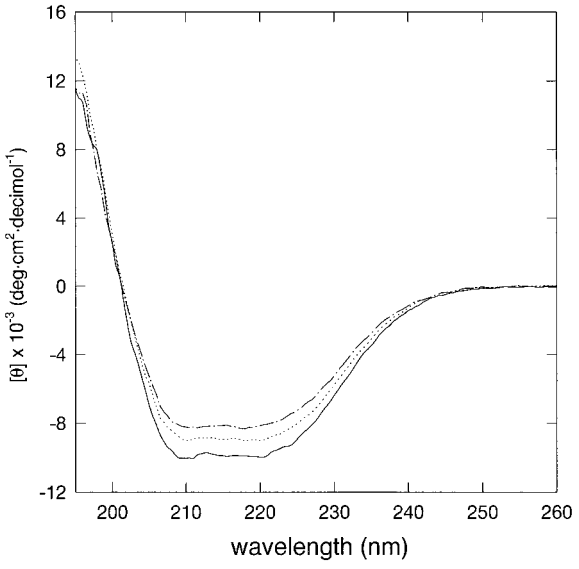

FIG. 4. **Effect of Mg^{2+} on the far-UV CD spectrum of GDP-tubulin (5 μM).** Each spectrum represents an average of four scans. Free Mg^{2+} concentrations are 1 mM (*solid line*), 3 μM (*dotted line*), and 65 nM (*dashed line*).

decrease with the Mg^{2+} concentration (4.0–5.5 $\times$ 10^{-5} s^{-1} at 60 nM, 2.5–3.0 $\times$ 10^{-5} s^{-1} at 300 nM, and 3.8–4.6 $\times$ 10^{-6} s^{-1} at 100 μM free Mg^{2+}).[2] As a control for sedimentation equilibrium measurements, the decay of MTC binding by tubulin was also measured at 10 °C in 65 nM free Mg^{2+}, giving an apparent first order constant of 0.9 $\times$ 10^{-5} s^{-1} ($t_{½}$ = 21 h; data not shown).

High Affinity Mg^{2+} Binding Enhances the Fluorescence of MTC Bound to the Colchicine Site of Tubulin—The addition of Mg^{2+} to the complex of the colchicine analogue MTC with tubulin, previously equilibrated at 50–60 nM free Mg^{2+}, leads in a few seconds to a large increase in the fluorescence of the ligand (Fig. 3). The variation is equivalent to the change in fluorescence observed upon MTC binding to GDP-tubulin with its Mg^{2+} high affinity site previously saturated with the cation. Control experiments indicated that Mg^{2+} affects neither the negligible fluorescence of unbound MTC nor the intrinsic (tryptophan) fluorescence of tubulin. Furthermore, Mg^{2+}-induced increase in the fluorescence of the MTC-tubulin complex cannot be explained in terms of variation in the extent of MTC binding to tubulin, since it was found to be independent of the free Mg^{2+} concentration (0.7 ± 0.1 MTC/tubulin heterodimer). The apparent association constant of Mg^{2+} to GDP-tubulin estimated from the MTC fluorescence change (Fig. 3) was 9 $\times$ 10^6 M^{-1}, essentially coincident with the association constant of the high affinity Mg^{2+} (Fig. 1). Mg^{2+} binding also increased the fluorescence of colchicine bound to tubulin, but only when the cation was bound prior to the addition of colchicine (data not shown). This different Mg^{2+} effect with MTC and colchicine might indicate that the slow dissociation rate of the latter prevents the ligation of Mg^{2+} to the N-site.

The simplest interpretation of these results is that the microenvironment of tubulin-bound MTC is sensitive to the high affinity bound Mg^{2+} ion, which actually induces the fluorescence of this colchicine site probe. Furthermore, the results also reveal communication between tubulin subunits, since the binding of the cation to N-site in α-tubulin modifies the properties of the colchicine site, whose locus is at the β-subunit, possibly near the $\alpha\beta$-subunit interface (56).

Modification of tubulin secondary structure upon removal of the high affinity bound Mg^{2+} was checked by CD spectroscopy. Equilibration of the protein in 65 nM free Mg^{2+} leads to a small reduction in the absolute magnitude of the dichroic signal at 210–220 nm (Fig. 4). The effect is independent of having GDP or GTP in the buffer, suggesting that the observed change is in part induced by Mg^{2+} coordination at the N-site. The analysis of this small change in the CD spectrum of tubulin indicated very small differences in the estimated secondary structure content. The CD change can be partially reversed by increasing the free Mg^{2+} concentration up to 1 mM (data not shown). Preliminary CD kinetic experiments of Mg^{2+} dissociation from tubulin and their subsequent reassociation, indicated that dissociation is slow (on the order of minutes), whereas reassociation is comparatively fast (on the order of seconds).

Role of Mg^{2+} in $\alpha\beta$-Tubulin Association—Cations bound with high affinity to oligomeric proteins frequently have structural roles, and their removal is linked to a marked weakening of protein-protein association equilibria (two examples are the platelet integrin $\alpha_{IIb}\beta_3$ (57) and the complement C1 subcomponent (48)). For this reason, the influence of Mg^{2+} (low and high affinity binding sites) on the dimerization equilibrium of tubulin was analyzed by analytical ultracentrifugation. GDP-tubulin equilibrated in 50–60 nM Mg^{2+}, at an initial protein concentration of 15 μM, has the same sedimentation coefficient ($s_{20,w}$ = 5.8 ± 0.2 S) and relative molecular mass (109,000 ± 8,000; Fig. 5) as the intact $\alpha\beta$-tubulin dimer. However, the tubulin dimer dissociation is patent at lower concentrations, as was analyzed by sedimentation equilibrium at 10 °C. Fig. 6 shows the variation in the average molecular mass of tubulin as a function of total tubulin and free Mg^{2+} concentrations. The results indicate that removal of Mg^{2+} from its high affinity site increases dissociation of the tubulin dimer. This behavior reflects the linkage of Mg^{2+} binding and tubulin self-association equilibria. Lowering the free Mg^{2+} concentration reduced by an order of magnitude the apparent equilibrium dimerization con-

[2] The first order fit does not account for the initial decay at 60 nM Mg^{2+}. The data are also compatible with a two-phase inactivation model (data not shown). This gives a fast phase ($t_{½}$ = 1.5 h) that practically starts from fully active cation-depleted tubulin at time zero (simultaneous with the initial nucleotide release, Table I) and a slow phase ($t_{½}$ = 15 h) that might consist of the inactivation of the remaining fraction of cation-containing tubulin.

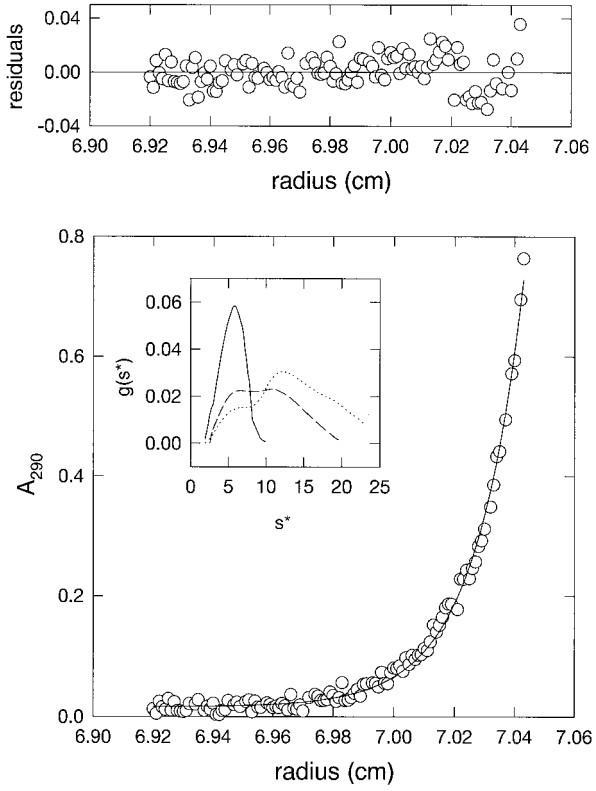

FIG. 5. **Analytical ultracentrifugation of GDP-tubulin at 50–60 nM free Mg^{2+} (10 °C).** Sedimentation equilibrium profile of tubulin under the conditions used in DSC experiments (15 μM loading protein concentration). *Inset*, sedimentation velocity distribution of tubulin samples. The *solid line* corresponds to the same tubulin showed in the main figure. The *dashed* and *dotted lines* are GDP-tubulin after 30 min at 40 °C and 60 °C, respectively.

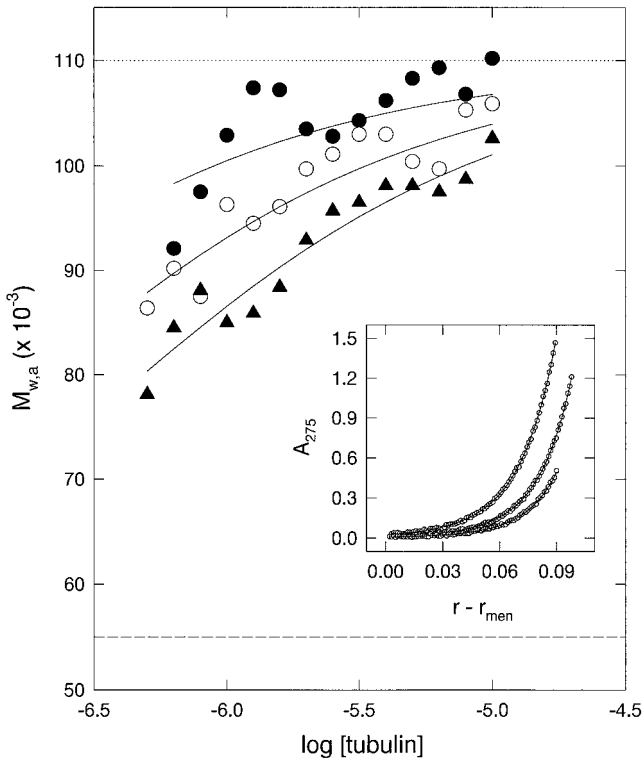

FIG. 6. **Influence of Mg^{2+} on the GDP-tubulin dimerization equilibrium.** Dependence of the apparent weight-average molecular mass of GDP-tubulin on free Mg^{2+} and protein concentration. Cation concentrations: 50 μM (*closed circles*), 1.6 μM (*open circles*), 60 nM (*solid triangles*). The *solid lines* were calculated for a monomer-dimer equilibrium model using the equilibrium constants given in Table II. For illustrative purposes, the M_r of α- and β-tubulin (55,000), as well as the value for the heterodimer (2 × 55,000) are indicated by the *dashed* and *dotted lines*, respectively. *Inset*, sedimentation equilibrium gradients of tubulin (loading protein concentrations: 1, 2.5, and 5 μM; 26,000 rpm and 10 °C) at 60 nM free magnesium. The *solid lines* represent the best-fit function (see Table II).

stant of $\alpha\beta$-tubulin (K_2), from ~10^7 M^{-1} at ~100 μM free cation, to 4×10^6 M^{-1} at 1–2 μM cation, and to 1.6×10^6 M^{-1} at 50 nM free cation (see Table II and Fig. 6).

The simplest interpretation of these results is that both the high affinity binding of one Mg^{2+} ion to the N-site and the binding of lower affinity cations stabilize the tubulin heterodimer. The data are compatible with the results obtained in the 10^{-3} to 10^{-4} M free Mg^{2+} concentration range by Shearwin *et al.* (8), who suggested the involvement of two weakly bound Mg^{2+} ions in the association of the GDP-tubulin heterodimer. A linked equilibria analysis of our data supports the notion that both low and high affinity Mg^{2+} enhance tubulin dimerization. As shown under "Appendix," the *combined* sedimentation equilibria data may be reasonably accounted for by a Mg^{2+}-dependent dimerization model, which is compatible with both the experimental dependence of K_2 on the cation concentration (Table II) and the Mg^{2+}-binding isotherm at high protein concentration (Fig. 1). According to this model, only one of the isolated subunits of GDP-tubulin bears a high affinity Mg^{2+} binding site, with an intrinsic binding constant of 2×10^6 M^{-1}, whereas the heterodimer has two independent Mg^{2+} binding sites, with binding constants 1×10^7 M^{-1} and 6×10^4 M^{-1}, respectively. The estimated value for the intrinsic dimerization constant of tubulin in the absence of Mg^{2+} is $K_2^0 = 10^6$ M^{-1}. The limited dissociation range of tubulin at the lowest protein concentration that could be measured in the analytical ultracentrifuge, as well as the need for avoiding the possible influence of tubulin denaturation processes at longer equilibrium times, preclude a more complete quantitative analysis in terms of linked functions (58, 59).

TABLE II
Effect of Mg^{2+} on the dimerization equilibrium of $\alpha\beta$-tubulin

Sample	$[Mg^{2+}]_{free}$	log K_2[a]	[95% confidence limits]
	M		
GDP-tubulin	4.0×10^{-8}	6.2	[6.1, 6.4]
GDP-tubulin	1.0×10^{-6}	6.5	[6.3, 6.6]
GDP-tubulin	2.0×10^{-6}	6.6	[6.5, 6.7]
GDP-tubulin	4.0×10^{-5}	7.1	[6.9, 7.5]
GDP-tubulin	6.3×10^{-4}	7.5	[7.3, —]
GTP-tubulin	5.0×10^{-5}	7.0	[6.9, 7.4]
GTP-tubulin	6.3×10^{-4}	7.2	[7.1, —]

[a] K_2 is the molar association constant.

Roles of Mg^{2+} and Nucleotide in the Thermal Stability of Tubulin—The influence of Mg^{2+} on the thermal stability of tubulin was analyzed by differential scanning calorimetry. Fig. 7*A* compares representative DSC profiles of GDP-tubulin in PEDTA buffer at increasing free Mg^{2+} concentrations. The experimental curves show that tubulin is strongly stabilized against thermally induced denaturation through interaction with the cation in the 10 nM to ~1 μM range of free ligand concentration. Above 1 μM free Mg^{2+}, the heat capacity curve presents a single asymmetric peak with an enthalpy change of 180 ± 10 kcal mol^{-1} and a T_m of 55 °C, whereas at the lower cation concentrations (25–40 nM free Mg^{2+}) the denaturation enthalpy change decreases to 130 ± 25 kcal mol^{-1}, and the endotherm tends to become separated into two peaks (Figs. 7*A* and 9*B*), the main one with a T_m of 46 °C at 25 nM free Mg^{2+}. The origin of the two peaks will be analyzed later.

Substitution of GDP by GTP at the E-site does not modify

tubulin stabilization by Mg^{2+}, which nearly reaches a plateau above 1 μM free Mg^{2+} (Fig. 7*B*). The results strongly suggest that the cation responsible for the substantial tubulin stabilization observed is the Mg^{2+} ion coordinated with the nucleotide N-site, since (i) the stabilization essentially coincides with the binding of this high affinity cation, (ii) the additional cation bound by GTP-tubulin has insignificant effect on the thermal stability of the protein, and (iii) the affinity of Mg^{2+} for the E-site in GDP-tubulin is known to be about 10^3 times lower than in GTP-tubulin (3, 4). Table III summarizes the parameters measured for the thermal denaturation of tubulin.

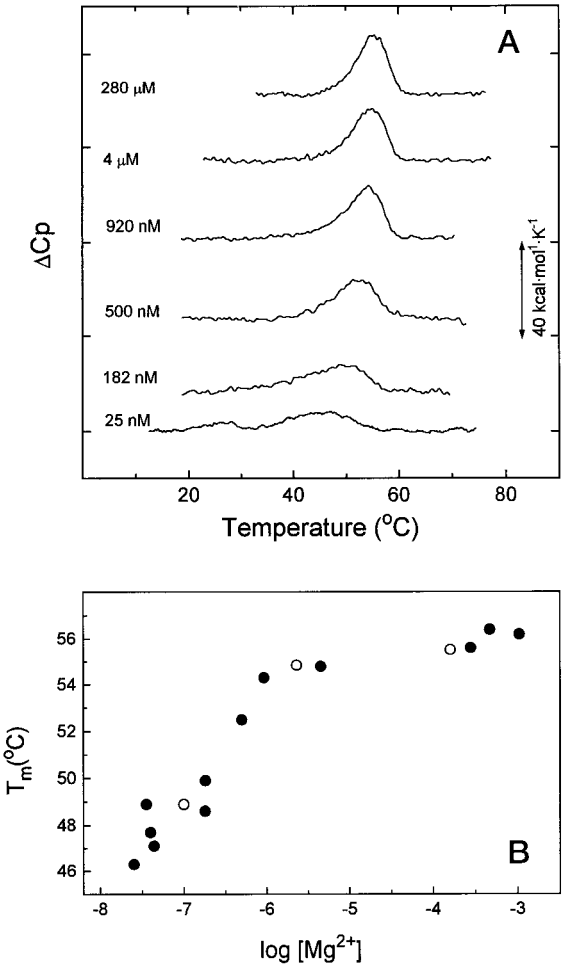

FIG. 7. *Panel A*, thermal denaturation curves of GDP-tubulin (15 μM) at increasing concentrations of Mg^{2+}. The experiments were done at a scan rate of 0.5 K·min^{-1}. Free Mg^{2+} concentrations (from top to bottom): 280 μM, 4 μM, 920 nM, 500 nM, 182 nM, and 50 nM. *Panel B*, dependence of denaturation T_m values of GDP-tubulin (15 μM) on the free Mg^{2+} concentration (*solid circles*); *open circles* correspond to GTP-tubulin.

The reversal of tubulin destabilization induced by Mg^{2+} depletion was checked by preparing protein samples equilibrated at different cation concentrations and then adding Mg^{2+} up to saturation (Table IV). The destabilization induced by the cation dissociation was 95% reversible in tubulin samples initially equilibrated in 180 nM free Mg^{2+} and immediately supplemented with 280 μM free Mg^{2+} (ΔH_d = 176 kcal mol^{-1}, T_m = 56.1 °C; Fig. 8, *curve b*). However, when Mg^{2+} was added after 2 h of incubation at 20 °C in the equilibration buffer, the shape of the calorimetric profile was indistinguishable from that obtained upon saturation with the cation immediately after protein elution, but the enthalpy change dropped to about 75% of the initial value (ΔH_d = 139 kcal·mol^{-1}; T = 56.1 °C; *curve c* in Fig. 8).The drop in ΔH_d observed after 2 h at 20 °C correlates with the value expected from the kinetics of tubulin inactivation under same conditions (Fig. 2). Reconstitution of tubulin samples initially prepared in 40 nM free Mg^{2+} (ν_{Mg} = 0.4, ν_{GTP} = 0.65) results in heat capacity denaturation curves with the same T_m value as in the control experiments but with a lower enthalpy change (142 kcal·mol^{-1}; *curve e*, Fig. 8). The percentage of reversibility obtained by saturation with Mg^{2+} immediately after preequilibration in Mg^{2+}-depleted buffers, correlates well with the initial GTP/tubulin stoichiometry of the samples. These results indicate that Mg^{2+}- or nucleotide-depleted tubulin slowly evolves in an irreversible way toward a state that does not undergo a temperature induced cooperative transition, and that GTP bound to the N-site of tubulin might determine the reversibility of Mg^{2+} dissociation. Addition of colchicine stabilized the cation-depleted tubulin, similarly to addition of Mg^{2+}, whereas the reversible binding of the colchicine analogue MTC had a much weaker effect (Table V).

Kinetic Control of the Thermal Denaturation of Tubulin by High Affinity Mg^{2+} Binding: Mechanism of Thermal Denaturation—Reheating of tubulin samples cooled after the first thermal scan showed that thermal denaturation of tubulin is irreversible under all the conditions tested. The thermograms depend on the scan rate (see Fig. 9, *A* and *B*) and the analysis of DSC curves showed that, on saturation of the high affinity Mg^{2+} binding site, the variation in the excess heat capacity with temperature follows the behavior predicted by the two-state kinetic model (53, 54). Fig. 9*C* shows the temperature dependence of the apparent denaturation rate constant at different free Mg^{2+}concentrations, calculated according to this model. This result means that only Mg^{2+} liganded (N-site) and denatured tubulin are significantly populated within the dena-

TABLE III
Thermal denaturation data of GDP- and GTP-tubulin at different free Mg^{2+} concentrations and scanning rates

	[Mg^{2+}]	Scan rate	T_1	ΔH_1	T_2	ΔH_2	ΔH_t
		°C · h^{-1}	*°C*	*kcal · mol^{-1}*	*°C*	*kcal · mol^{-1}*	*kcal · mol^{-1}*
GDP-tubulin	25 nM	30	25.9	35	46.3	119	156
GDP-tubulin	35 nM	30	23.7	38	48.9	84	122
GDP-tubulin	50 nM	45	31.5	20	50.1	73	93
GDP-tubulin	30 nM	60	—[a]	—	51.1	160	160
GDP-tubulin	40 nM	60	35.0	31	52.0	84	113
GDP-tubulin	75 nM	90	24.2	14	54.8	133	147
GDP-tubulin	182 nM	30	—	—	49.9	158	158
GDP-tubulin	500 nM	30	—	—	52.5	172	172
GDP-tubulin	927 nM	30	—	—	54.5	185	185
GDP-tubulin	4.5 μM	30	—	—	54.8	173	173
GDP-tubulin	280 μM	30	—	—	55.6	186	186
GDP-tubulin	280 μM	20	—	—	54.2	200	200
GTP-tubulin	2.3 μM	30	—	—	54.6	173	173
GTP-tubulin	160 μM	30	—	—	55.8	150	150

[a] —, not observed in third sample and not applicable in seventh to fourteenth samples.

TABLE IV
Reversibility of thermal destabilization induced by Mg^{2+} removal from GDP-tubulin

$[Mg^{2+}]_{initial}$	$[Mg^{2+}]_{final}$	t	T_m	ΔH	$\Delta H_t/\Delta H_{control}$
nM	*μM*	*h*	*°C*	*kcal · mol⁻¹*	
180	280	0.5	56.1[a]	176	0.98[c]
180	280	2	56.1	139	0.77
40–50	470	0.5	58.2[b]	136	0.75

[a] Scan rate, 30 °C · h^{-1}.
[b] Scan rate, 45 °C · h^{-1}.
[c] $\Delta H_{control}$ was taken as 180 kcal · mol^{-1}.

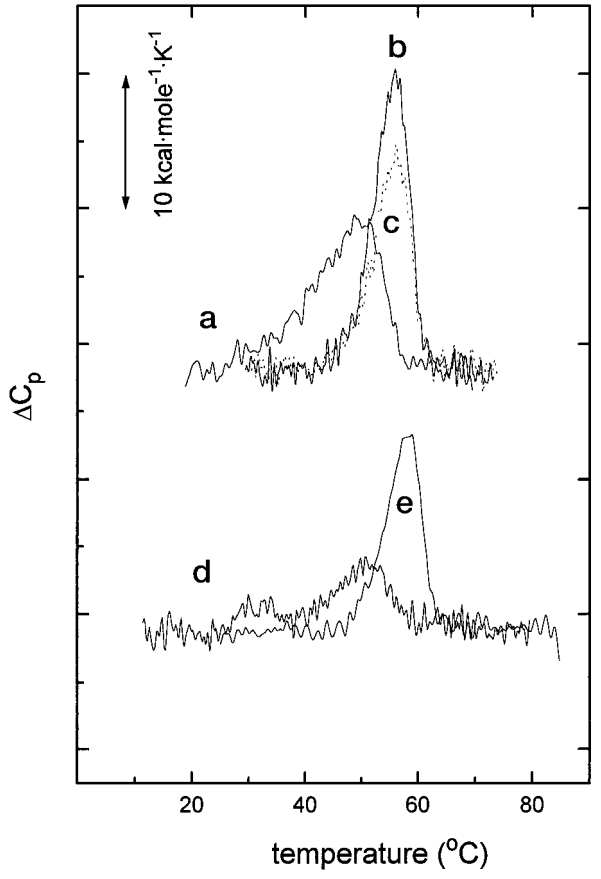

FIG. 8. **Reversibility of the Mg^{2+} stabilizing effect on thermal denaturation of GDP-tubulin (15 μM).** *Curve a*, endotherm of tubulin equilibrated at 180 μM free Mg^{2+}; *curve b*, the same as *a* but supplemented with Mg^{2+} (280 μM final free concentration) immediately after column elution; *curve c*, the same as *a* but supplemented with Mg^{2+} after incubation for 2 h at 20 °C (scan rate 30 °C·h^{-1}); *curve d*, endotherm of GDP-tubulin equilibrated at 45 nM free Mg^{2+}; *curve e*, the same as *d*, but supplemented up to 470 μM free Mg^{2+} immediately after elution from the preparative column (scan rate 45 °C·h^{-1}).

turation temperature range. A good correlation was found between the kinetic constants of inactivation calculated from the rate of CD change at 55 °C (θ_{220}, free $[Mg^{2+}]$ = 180 nM) or from DSC data at the same temperature and cation concentration (3×10^{-3} s^{-1} and 3.5×10^{-3} s^{-1}, respectively). However, the kinetic constants extrapolated from the DSC data to 20 °C are several orders of magnitude smaller than those measured from tubulin inactivation at this temperature, suggesting a different origin for the two processes in the lower temperature range.

At the lowest free Mg^{2+}concentrations (40–100 nM), the denaturation process becomes complex as indicated by the presence of a shoulder or small peak in the low temperature side (Figs. 7–9). This is also evident in the loss of secondary structure, monitored by CD at 220 nm (Fig. 10).The enthalpy change associated with the low temperature shoulder can be roughly

TABLE V
Influence of MTC and colchicine on GDP-tubulin stability

Ligand	$[Mg^{2+}]^a$	T_m	ΔH
		°C	*kcal · mol⁻¹*
	182 nM	49.9	158
MTC	182 nM	51.0	133
Colchicine	182 nM	54.6	191
	4.5 μM	54.8	173
MTC	4.5 μM	54.5	170
Colchicine	4.5 μM	56.5	189

[a] Tubulin was equilibrated in 182 nM free Mg^{2+}, optionally supplemented to 4.5 μM free Mg^{2+}, and 100 μM MTC or 100 μM colchicine added. Scan rate was 30 °C · h^{-1}.

estimated to be ~30 ± 5 kcal·mol^{-1}. The CD spectra of thermally denatured tubulin has residual β sheet secondary structure (60). The apparent biphasic denaturation of tubulin at subsaturating levels of Mg^{2+} could be generated by different processes such as kinetic stabilization of unfolding intermediates, uncoupling of α- and β-subunit denaturation, or association of the denatured state. In addition, given the slow dissociation of the nucleotide from tubulin and the presence of GTP at substoichiometric ratios under these conditions (61–63), the low and high temperature peaks could also derive from the unligated and nucleotide-bound tubulin, respectively.

Sedimentation velocity measurements have shown that the association state of thermally denatured tubulin depends on the Mg^{2+} concentration. Incubation of GDP-tubulin equilibrated in 50 nM free Mg^{2+} at 40 °C for 30 min induces a partial aggregation of tubulin, giving a bimodal sedimentation velocity profile, in which approximately half of the protein sediments as the tubulin dimer ($s_{20,w}$ = 5.7 S) and the other half as a 12 S oligomer (see *dotted line* in the *inset* of Fig. 5). Furthermore, 30-min incubation at 60 °C results in a higher percentage (~70%) of tubulin aggregation (13–14 S). However, when the same treatment was performed on GDP-tubulin with the high affinity site occupied by Mg^{2+}, aggregation was not evident ($s_{20,w}$ = 5.9 S). These results suggest that tubulin aggregation might be involved in the generation of the biphasic denaturation curves. Nevertheless, contributions from other processes (see above) cannot be ruled out. A possible minimal scheme to account for thermal denaturation of tubulin at the Mg^{2+} concentration range explored is as follows.

$$\begin{array}{ccccc} \mathrm{TB + GTP + Mg^{2+}} & \overset{K^{\alpha}_{GTP}}{\rightleftharpoons} & \mathrm{TB \cdot GTP + Mg^{2+}} & \overset{K^{\alpha}_{Mg}}{\rightleftharpoons} & \mathrm{TB \cdot GTP \cdot Mg^{2+}} \\ \uparrow\downarrow & & \uparrow\downarrow & & \\ X_1 & & X_2 & & \downarrow k_3 \\ \downarrow k_1 & & \downarrow k_2 & & \\ I_1 & & I_2 + \mathrm{GTP} & & I_3 + \mathrm{GTP} + \mathrm{Mg^{2+}} \end{array}$$

SCHEME 1

K^{α}_{GTP} and K^{α}_{Mg} are the GTP and Mg^{2+} binding constants to N-site, k_3 is the denaturation rate constant of tubulin·GTP·Mg, and k_1 and k_2 are the limiting rate constants for denaturation of N-site unliganded and GTP-bound tubulin, respectively; I_i are irreversibly denatured state(s) of tubulin (I_1 and I_2 are 12–14 S aggregated species, and I_3 is 5.9 S denatured tubulin) and X_i indicates the possibility of intermediate steps during denaturation.

CONCLUSION

The results reported in this study provide new insights into tubulin structure and function. This is schematically summarized in Fig. 11. The nucleotide γ-phosphate and the coordinated Mg^{2+} ion at the E-site (β) of tubulin, which regulate the tubulin assembly function and microtubule stability, have practically undetectable effects on the stability and on most of the solution properties of the αβ-tubulin dimer. However, one

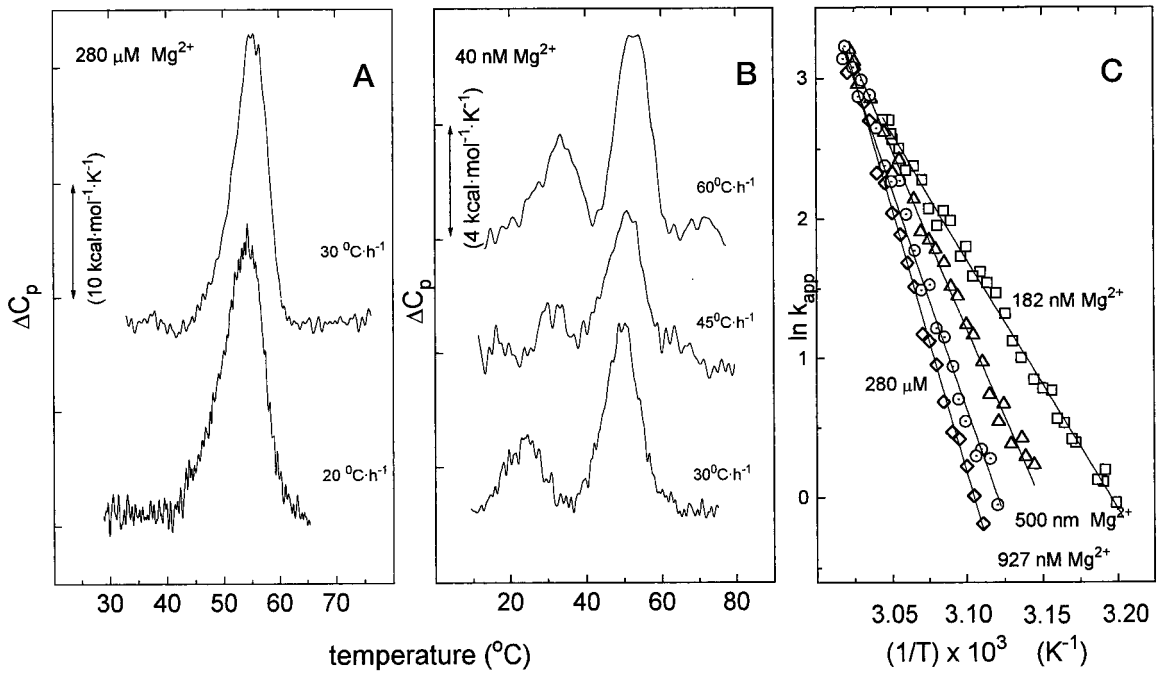

FIG. 9. *Panels A* and *B*, DSC traces of GDP-tubulin (15 μM) at different scanning rates and free Mg^{2+} concentrations. *Panel A*, 280 μM free Mg^{2+} (30 and 20 °C·h^{-1}; top to bottom). *Panel B*, 40 nM free Mg^{2+} (60, 45, and 30 °C·h^{-1}; from top to bottom). *Panel C*, Arrhenius plot of the kinetic rate constant, k_{app}, derived from calorimetric data assuming the two-state kinetic model, at different free Mg^{2+} concentrations: 280 μM (*diamonds*), 927 nM (*circles*), 500 nM (*triangles*), and 182 nM (*squares*).

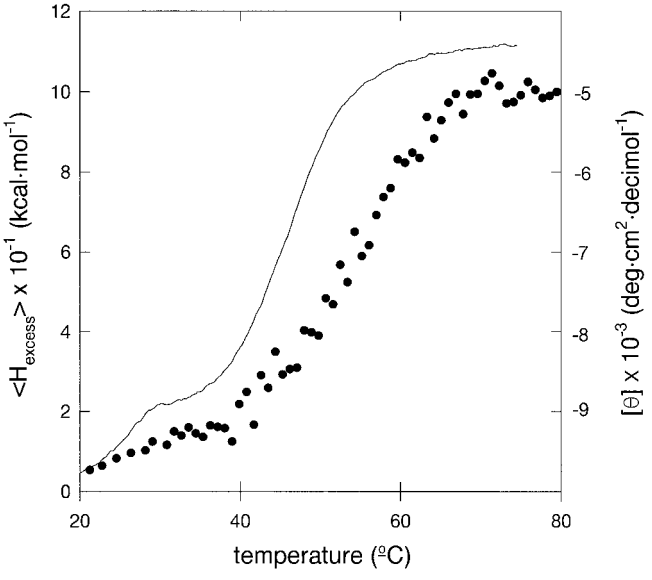

FIG. 10. **Dependence of the excess enthalpy function (H_{excess}) and the CD signal at 220 nm (θ_{220}) of tubulin with temperature (65 nM free Mg^{2+}).** The *solid line* shows the excess enthalpy values of the corresponding DSC curve. The *symbols* show the experimental CD data. Tubulin concentration was 15 μM and the temperature scan rate 0.5 °C min^{-1}.

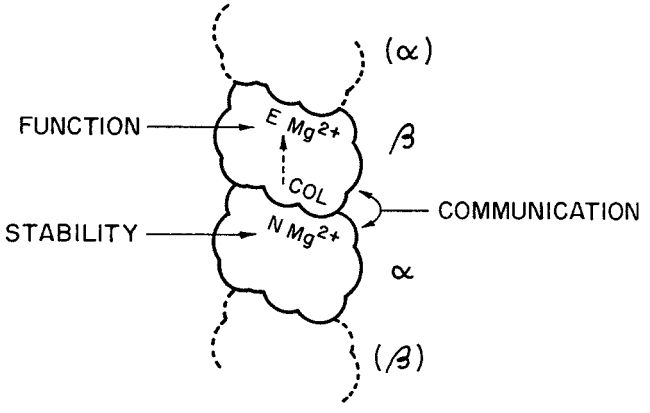

FIG. 11. **Model scheme proposed to explain and summarize the results of this work.** The nucleotide and Mg^{2+} bound to the E-site, which are known to regulate the tubulin assembly function, have insignificant effects on the stability of tubulin. The high affinity Mg^{2+} ion bound at the nucleotide N-site controls the stability of the $\alpha\beta$-tubulin dimer. The simplest explanation for the observed effect of the Mg^{2+} binding at the N-site on the fluorescence of a probe bound to the colchicine site (*COL*) is close communication, *i.e.* both sites being near the α-β dimerization interface. It follows that nucleotide-Mg^{2+} E-site should be at the interface of association of the dimer with the next dimer along one protofilament of the microtubule. The *dashed arrow* from the colchicine site to E-site indicates the allosteric communication, which activates the GTPase activity in the $\alpha\beta$-dimer upon colchicine binding, although the sites are more than 2.4 nm apart (for this and other distances, see Ref. 66). The shape of the tubulin dimer corresponds to a contour view from the outside of a low resolution microtubule model deduced from x-ray solution scattering (67).

high affinity Mg^{2+} ion, bound to a site identified as the nonfunctional nucleotide N-site (α), has profound kinetic and thermal stabilizing effects, and induces the association of the $\alpha\beta$-dimer. The α- and β-subunits seem to communicate with each other; the binding of Mg^{2+} to the N-site in the α-subunit induces the fluorescence of a probe bound to the colchicine site in the β-subunit, and colchicine binding thermally stabilizes Mg^{2+}-depleted tubulin. These properties are most simply explained by proposing that both the colchicine site (β) (56) and the N-site Mg^{2+} (α) (this study) are located at the $\alpha\beta$ dimerization interface. It follows from subunit homology that the functional E-site (in β) should be at the longitudinal dimer-dimer interface leading to protofilament formation (64), consistent with the activation of tubulin GTPase in linear oligomers (65).

All tubulins probably evolved from a common nucleotide-binding ancestor. The GTP and Mg^{2+} binding functionalities were made essential for the maintenance of the protein stability in α-tubulin, whereas β-tubulin acquired the capability to

hydrolyze bound GTP upon activation by proper contact with other tubulin molecules, which is the basic mechanism controlling microtubule stability. The sites of binding of the antimitotic drugs colchicine, vinblastine, and paclitaxel, for which endogenous ligands are unknown, are also primarily located in β-tubulin. It is presently unclear how a dimer was selected to assemble microtubules.

Acknowledgment—We thank Victoria Lopez Moyano for able technical assistance.

APPENDIX

Tubulin exists as an equilibrium mixture of monomers (α- and β- subunits) and dimers (αβ-heterodimer), with molecular weights M_α, M_β, and $M_{\alpha\beta}$, respectively ($M_\alpha = M_\beta$). The equilibrium dimerization constant, K_2, is shown in Equation 1 below.

$$\alpha + \beta \overset{K_2}{\rightleftharpoons} \alpha\beta \qquad K_2 = c_{\alpha\beta}/(c_\alpha \cdot c_\beta)$$

c_α, c_β, and $c_{\alpha\beta}$ represent the concentrations of the different forms in dilute solution, expressed in molar units.

The total concentration of tubulin, c_{tot}, and the weight-average molecular weight are given by Equations 2 and 3, respectively:

$$c_{tot} = c_\alpha + c_\beta + 2c_{\alpha\beta} \quad \text{(Eq. 1)}$$

$$M_{w,a} = \sum(c_j \cdot M_{wj}^2)/\sum(c_j \cdot M_{wj}) \quad \text{(Eq. 2)}$$

j represents any tubulin species (α, β, or αβ).

A simple general model of Mg^{2+} binding to tubulin assumes multiple classes of independent binding sites in any of the tubulin species. The Mg^{2+} binding isotherms for the α- and β-subunits and the αβ-heterodimer are given in Equations 4–6.

$$\nu_\alpha = \sum n_{\alpha i} \cdot K_{\alpha i} \cdot [Mg^{2+}]/(1 + K_{\alpha i} \cdot [Mg^{2+}]) \quad \text{(Eq. 3)}$$

$$\nu_\beta = \sum n_{\beta i} \cdot K_{\beta i} \cdot [Mg^{2+}]/(1 + K_{\beta i} \cdot [Mg^{2+}]) \quad \text{(Eq. 4)}$$

$$\nu_{\alpha\beta} = \sum n_{\alpha\beta i} \cdot K_{\alpha\beta i} \cdot [Mg^{2+}]/(1 + K_{\alpha\beta i} \cdot [Mg^{2+}]) \quad \text{(Eq. 5)}$$

ν_α, ν_β, and $\nu_{\alpha\beta}$ are the number of moles of Mg^{2+} bound per mole of isolated α- and β-subunits and tubulin heterodimer, respectively; n_{ji} and K_{ji} are the number of sites and the intrinsic association constant for the class i of binding sites in the isolated monomers or heterodimer (j = α, β, or αβ). The global binding isotherm is given in Equation 7.

$$\nu_{tot} = [c_\alpha \cdot \nu_{1\alpha} + c_\beta \cdot \nu_{1\beta} + c_{\alpha\beta} \cdot \nu_{2\alpha\beta}]/c_{tot} \quad \text{(Eq. 6)}$$

The apparent dimerization constant K_2 at a given ligand concentration, $[Mg^{2+}]$, may be expressed, in terms of linked equilibria theory (48, 58), by Equation 8.

$$\log K_2 = \log K_2^0 + \sum n_{\alpha\beta i} \cdot \log(1 + K_{\alpha\beta i} \cdot [Mg^{2+}]) - \{\sum n_{\alpha i} \cdot \log(1 + K_{\alpha i} \cdot [Mg^{2+}] + \sum n_{\beta i} \cdot \log(1 + K_{\beta i} \cdot [Mg^{2+}])\} \quad \text{(Eq. 7)}$$

From this, Equation 9 can be derived.

$$d(\log K_2)/d(\log[Mg^{2+}]) = \nu_{\alpha\beta} - (\nu_\beta + \nu_\alpha) \quad \text{(Eq. 8)}$$

To obtain the number of binding sites and the equilibrium binding constants for each subunit and the heterodimer, the value of M_w as a function of tubulin and Mg^{2+} concentration were determined in the following way. The equilibrium constant, K_2, was calculated from Equation 8, given the values of K_2^0, $[Mg^{2+}]$, and c_{tot}, together with the values of n_{ji} and K_{ji} for the different species. The values of c_α and c_β were determined by solving Equations 1 and 2. Finally, Equation 3 was used to calculate M_w. The global binding isotherm was then obtained from Equation 7.

Using this analytical procedure, different models were fitted to the combined $M_{w,a}$ *versus* concentration data (derived from nine sedimentation equilibrium gradients, at three initial concentrations of tubulin and Mg^{2+}; see Fig. 6). In all of them, the

TABLE VI
Models of Mg^{2+}-linked dimerization applied to the combined sedimentation equilibrium data
Data from Fig. 6 are shown.

Model	α-Subunit, n_{11}	β-Subunit, n_{11}	αβ-Tubulin 1st class, n_{21}	αβ-Tubulin 2nd class, n_{22}
1	0	0	1	0
2[a]	1	0	1	0
3[a]	1	0	1	1
4	1	1	1	1
5	1	1	1	2

[a] Only one subunit (α or β) has a Mg^{2+} binding site (for simplicity, it is shown in the α subunit).

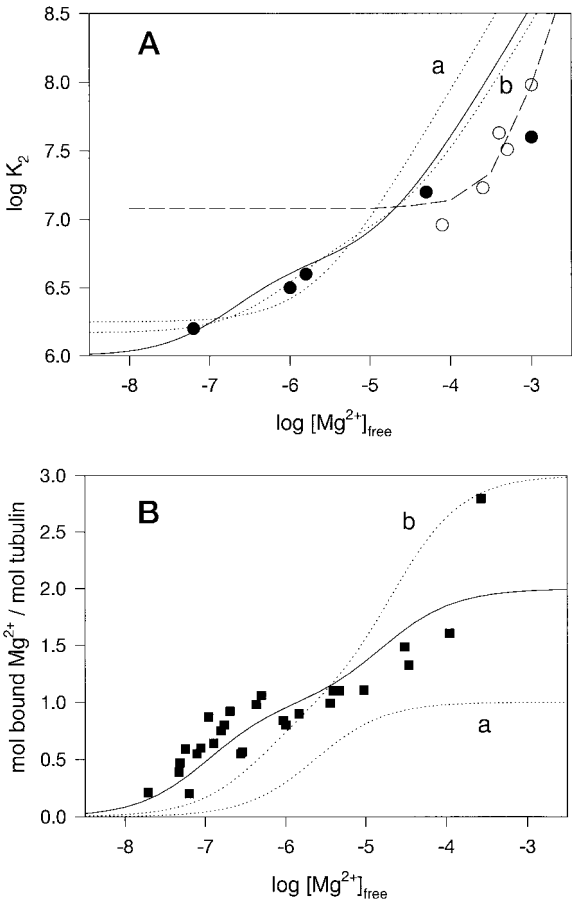

FIG. 12. **Linkage between Mg^{2+} binding and tubulin dimerization.** *Panel A*, dependence of the tubulin dimerization constant on free Mg^{2+} concentration. *Symbols* correspond to dimerization constants determined from sedimentation equilibrium data in the present work (*solid circles*; Table II), compared with those obtained by Shearwin and Timasheff (*open circles*; Ref. 56). The *solid line* corresponds to the theoretical values calculated from Equation 7, using the parameters of the best model described in the text (see model 3 in Table VI). The *dashed line* corresponds to the data and model of Shearwin and Timasheff (see Equation 7 in Ref. 56). The *dotted lines* show the calculated functions from models 1 (*curve a*) and 5 (*curve b*) (see Table VI). *Panel B*, number of Mg^{2+} ions bound per tubulin as a function of free Mg^{2+} concentration. *Solid squares* are the experimental data (see Fig. 1). *Lines*, binding isotherms calculated for the linkage models and parameters described in the text; *solid line*, model 3 (best fit); *dotted lines*, models 1 (*curve a*) and 5 (*curve b*) (see Table VI).

ligand stoichiometry of the subunits and the heterodimer was constrained, the fitting parameters being K_2^0 and the different K_{ji} (see Table VI). These models were compatible with the sedimentation equilibrium gradients. The goodness of the fit was assessed by comparison of: (i) the calculated K_2 *versus* $[Mg^{2+}]$ curves with the experimental data (Fig. 12*A*) and (ii) the theoretical with the experimental binding isotherms (Fig. 12*B*). The best fit to the experimental values was obtained with a single binding site in one of the isolated subunits ($K_{11} = 2 \times 10^6\ M^{-1}$), two independent sites in the tubulin heterodimer ($K_{21} = 1 \times 10^7\ M^{-1}$, $K_{22} = 6 \times 10^4\ M^{-1}$), and a dimerization constant in the absence of Mg^{2+}, K_2^0, of $\sim 10^6\ M^{-1}$. Note that the deviation observed above 0.1 mM free Mg^{2+} in the binding isotherm should probably arise from the existence of several low affinity binding sites.

REFERENCES

1. de Pereda, J. M., Leynadier, D., Evangelio, J. E., Chacon, P., and Andreu, J. M. (1996) *Biochemistry* **35,** 14203–14215
2. Weisenberg, R. C., Borisy, G. G., and Taylor, E. W. (1968) *Biochemistry* **7,** 4466–4479
3. Correia, J. J., Baty, L. T., and Williams, R. C., Jr. (1987) *J. Biol. Chem.* **262,** 17278–17284
4. Correia, J. J., Beth, A. H., and Williams, R. C., Jr. (1988) *J. Biol. Chem.* **263,** 10681–10686
5. Carlier, M. F. (1991) *Curr. Opin. Cell Biol.* **3,** 12–17
6. Drechsel, D. N., and Kirschner, M. W. (1994) *Curr. Biol.* **4,** 1053–1061
7. Díaz, J. F., and Andreu, J. M. (1993) *Biochemistry* **32,** 2747–2755
8. Shearwin, K. E., Perez-Ramirez, B., and Timasheff, S. N. (1994) *Biochemistry* **33,** 885–893
9. Barbier, P., Peyrot, V., Leynadier, D., and Andreu, J. M. (1998) *Biochemistry*, in press
10. Howard, W. D., and Timasheff, S. N. (1986) *Biochemistry* **25,** 8292–8300
11. Díaz, J. F., Pantos, E., Bordas, J., and Andreu, J. M. (1994) *J. Mol. Biol.* **238,** 214–223
12. Melki, R., Carlier, M. F., Pantaloni, D., and Timasheff, S. N. (1989) *Biochemistry* **28,** 9143–9152
13. Hyman, A. A., and Karsenti, E. (1996) *Cell* **84,** 410–420
14. Spiegelman, B. M., Penningroth, S. M., and Kirschner, M. W. (1977) *Cell* **12,** 587–600
15. Carlier, M. F., Didry, D., and Valentin-Ranc, C. (1991) *J. Biol. Chem.* **266,** 12361–12368
16. Grover, S., and Hamel, E. (1994) *Eur. J. Biochem.* **222,** 163–172
17. Frigon, R. P., and Timasheff, S. N. (1975) *Biochemistry* **14,** 4559–4566
18. Frigon, R. P., and Timasheff, S. N. (1975) *Biochemistry* **14,** 4567–4573
19. Lee, J. C., and Timasheff, S. N. (1975) *Biochemistry* **14,** 5183–5187
20. Croom, H. B., Correia, J. J., Baty, L. T., and Williams, R. C. (1985) *Biochemistry* **24,** 768–775
21. Buttlaire, D. H., Czuba, B. A., Stevens, T. H., Lee, Y. C., and Himes, R. H. (1980) *J. Biol. Chem.* **255,** 2164–2168
22. Jemiolo, D. K., and Grisham, C. M. (1982) *J. Biol. Chem.* **257,** 8148–8152
23. Mejillano, M. R., and Himes, R. H. (1991) *Arch. Biochem. Biophys.* **291,** 356–362
24. Osei, A. A., Everett, G. W., and Himes, R. H. (1990) *FEBS Lett.* **276,** 85–87
25. Díaz, J. F., Menéndez, M., and Andreu, J. M. (1993) *Biochemistry* **32,** 10067–10077
26. Fabiato, A., and Fabiato, F. (1979) *J. Physiol.* **75,** 463–505
27. Bartfai, T. (1979) *Adv. Cyclic Nucleotides Res.* **10,** 219–242
28. Dawson, R. M. C., Elliot, D. C., Elliot, W. H., and Jones, K. M. (1986) *Data for Biochemical Research*, 3rd Ed., p. 404, Clarendon Press, Oxford
29. Tabor, H., and Hastings, A. B. (1943) *J. Biol. Chem.* **148,** 627–632
30. Greenwald, I., Redish, J., and Kibrick, A. L. (1940) *J. Biol. Chem.* **135,** 65–76
31. Courtney, R. C., Chabereck, S., and Martell, A. E. (1953) *J. Am. Chem. Soc.* **75,** 4814–4818
32. Sillén, L. G., and Martell, A. E. (1971) *Stability Constants of Metal Ion Complexes*, 2nd Ed., Burlington House, London
33. Klotz, I. M. (1985) *Q. Rev. Biophys.* **18,** 227–258
34. Press, W. H., Flannery, B. P., Teukolsky, S. A., and Vetterling, W. T. (1989) *Numerical Recipes in Pascal: The Art of Scientific Computing*, Cambridge University Press, Cambridge, MA
35. Menéndez, M., Gasset, M., Laynez, J., López-Zúmel, C., Usobiaga, P., Töffer-Petersen, E., and Calvete, J. J. (1995) *Eur. J. Biochem.* **234,** 887–896
36. Yang, J. T., Chuen-Shang, C. W.,and Martinez, H. M. (1986) *Methods Enzymol.* **130,** 208–269
37. Perczel, A., Park, K., and Fasman, G. D. (1992) *Anal. Biochem.* **203,** 83–93
38. Perczel, A., Park, K., and Fasman, G. D. (1992) *Proteins* **13,** 57–69
39. Andreu, J. M., Gorbunoff, M. J., Lee, J. C., and Timasheff, S. N. (1984) *Biochemistry* **23,** 1742–1752
40. Sackett, D. L., and Lippoldt, R. E. (1991) *Biochemistry* **30,** 3511–3517
41. Minton, A. P. (1994) in *Modern Analytical Ultracentrifugation* (Schuster, T. M., and Laue, T. M., eds) pp. 81–93, Birkhauser, Boston
42. Lee, J. C., and Timasheff, S. N. (1977) *Biochemistry* **16,** 1754–1764
43. Laue, T. M., Shah, B. D., Ridgeway, T. M., and Pelletier, S. L. (1992) in *Analytical Ultracentrifugation in Biochemistry and Polymer Science* (Harding, S. E., Rowe, A. J., and Horton, J. C., eds) pp. 90–125, Royal Society of Chemistry, Cambridge, United Kingdom
44. Johnson, M. L., Correia, J. J., Yphantis, D. A., & Halvorson, H. R. (1981) *Biophys. J.* **36,** 575–588
45. Andreu, J. M., and Timasheff, S. N. (1982) *Biochemistry* **21,** 6465–6476
46. Lee, J. C., Frigon, R. F., and Timasheff, S. N. (1973) *J. Biol. Chem.* **248,** 7253–7262
47. Chatelier, R. C., and Minton, A. P. (1987) *Biopolymers* **26,** 507–524
48. Rivas, G., Ingham, K. C., and Minton, A. P. (1992) *Biochemistry* **31,** 11707–11712
49. Stafford, W. F., III (1992) *Anal. Biochem.* **203,** 295–301
50. Stafford, W. F. (1994) *Methods Enzymol.* **240,** 478–501
51. van Holde, K. E. (1986) *Physical Biochemistry*, 2nd Ed., pp. 110–121, Prentice Hall Inc., NJ
52. Arriaga, P., Menéndez, M., Martín Villacorta, J., and Laynez, J. (1992) *Biochemistry* **31,** 6603–6608
53. Sánchez-Ruíz, J. M., López-Lacomba, J. L., Cortijo, M., and Mateo, P. L. (1988) *Biochemistry* **27,** 1648–1652
54. Sánchez-Ruíz, J. M. (1992) *Biophys. J.* **61,** 921–935
55. Menéndez, M., Laynez, J., Medrano, F. J., and Andreu, J. M. (1989) *J. Biol. Chem.* **264,** 16367–16371
56. Shearwin, K. E., and Timasheff, S. N. (1994) *Biochemistry* **33,** 894–901
57. Rivas, G., Usobiaga, P., and González-Rodríguez, J. (1991) *Eur. Biophys J.* **20,** 287–292
58. Record, M. T., Jr., Anderson, C. F., and Lohman, T. M. (1978) *Q. Rev. Biophys.* **11,** 103–178
59. Wyman, J., and Gill, S. J. (1990) *Binding and Linkage: Functional Chemistry of Biological Macromolecules*, University Science Books, Mill Valley, CA
60. Mozo-Villarias, A., Morros, A., and Andreu, J. M. (1991) *Eur. Biophys. J.* **19,** 295–300
61. Brandts, J. F., and Lin, L.-N. (1990) *Biochemistry* **29,** 6927–6940
62. Shrake, A., and Ross, P. (1990) *J. Biol. Chem.* **265,** 5055–5059
63. Shrake, A., and Ross, P. (1992) *Biopolymers* **32,** 925–940
64. Kirchner, K., and Mandelkow, E. M. (1985) *EMBO J.* **4,** 2397–2402
65. Carlier, M. F., Didry, D., and Pantaloni, D. (1997) *Biophys. J.* **73,** 418–427
66. Ward, L. D., Seckler, R., and Timasheff, S. N. (1994) *Biochemistry* **33,** 11900–11908
67. Andreu, J. M., Bordas, J., Díaz, J. F., García de Ancos, J., Gil, R., Medrano, F. J., Nogales, E., Pantos, E., and Towns-Andrews, E. (1992) *J. Mol. Biol.* **226,** 169–184